

The window Josephson junction: a coupled linear nonlinear system

A. Benabdallah ^a, J. G. Caputo ^b and N. Flytzanis ^c

^a *Max-Planck-Institut für Physik komplexer Systeme, Nöthnitzer Straße 38, D-01187 Dresden, Germany*

^b *Laboratoire de Mathématique, INSA de Rouen, B.P. 8, 76131 Mont-Saint-Aignan cedex, France*

^c *Department of Physics, University of Crete, GR-71409, Heraklion, Greece.*

Abstract:

We investigate the interface coupling between the 2D sine-Gordon equation and the 2D wave equation in the context of a Josephson window junction using a finite volume numerical method and soliton perturbation theory. The geometry of the domain as well as the electrical coupling parameters are considered. When the linear region is located at each end of the nonlinear domain, we derive an effective 1D model, and using soliton perturbation theory, compute the fixed points that can trap either a kink or antikink at an interface between two sine-Gordon media. This approximate analysis is validated by comparing with the solution of the partial differential equation and describes kink motion in the 1D window junction. Using this, we analyze steady state kink motion and derive values for the average speed in the 1D and 2D systems. Finally we show how geometry and the coupling parameters can destabilize kink motion.

Keywords: solitons, Josephson junctions, sine-Gordon, wave equation.

1 Introduction

Nonlinear wave equations in one dimension that are close to integrable have been studied extensively for the past twenty years. The shift from exact integrability can be due to the presence of extra terms in the equation or to an additional evolution equation. In the former case perturbation methods give good results. This kind of approach is far more difficult when two such equations are coupled. In that case one needs to resort to extensive numerical studies in order to gain insight and develop approximate models. This is also true when one uses realistic boundary conditions, such as an impedance condition.

Here we consider a 2D sine-Gordon equation coupled to a 2D wave equation via interface conditions. Such a model was originally derived for a so-called window Josephson junction [1,2] between two superconductors where the thickness of the oxide layer is small in the junction area and larger in the surrounding region. The electrodynamics of such a system is described by the sine-Gordon equation in the window area [3] where tunneling of electron pairs is possible and by the wave equation in the surrounding passive region. This model is much more general and could describe the motion of dislocations in a stressed inhomogeneous thin plate [4], in this case the on site potential would be non uniform. Another example is the motion of domain walls in a one dimensional inhomogeneous ferromagnet [5]. One could also generalize the 2D rotator array of [6]. From a fundamental point of view, the window junction allows to study in detail the interactions between a linear and a nonlinear system. The relation between the two subsystems can be changed by using a different geometry or topology or by modifying the coupling parameters. In the case of the Josephson junction, the former are the junction inductance and capacitance per unit area.

Let us now recall what has been done to solve this problem. For static solutions the longitudinal extension of the passive region has been shown not to play a big role, only the lateral extension changes the solution [7]. For small extensions w' , the length of the problem is rescaled from λ_J into $\lambda_{\text{eff}} = \sqrt{1 + 2\frac{w'}{w} \frac{L_J}{L_I}}$ [7] where L_J (resp. L_I) is the inductance in the junction (resp. passive region).

This rescaling explains very well the static solutions in the presence of a magnetic field [8], it is a local effect which can also be seen for annular geometries [9]. For very large passive regions, the kink width is proportional to the inverse of the width of the junction, it can be very big and cause the destruction of the kink due to the longitudinal junction boundaries[1]. This could explain the absence of fluxon motion in window junctions with large passive regions.

Lee and co-workers [10,11] investigated an infinite linear superconducting strip line where no Josephson current is present. They obtained the dispersion relation indicating that waves can propagate in the x direction and have a transverse structure in y. This study done in the linear case does not give any indications on the effect of the linear passive region on kinks which are strongly nonlinear. Another issue is that this analysis is based on eigenmodes and cannot be extended to the case when there is an external current applied to the device.

In [12] experiments have been conducted on Fiske steps in window junctions with two different geometries a lateral passive region and longitudinal passive region. Lumped elements were assumed and simple models were derived from which the velocity was obtained. A passive region placed at each end of the junction acts as a lumped capacitance and generates radiation. On the contrary a passive region placed along the junction acts as a transmission line in parallel to the junction. It gives a rescaling of the Josephson penetration length and a larger fluxon rest mass in agreement with [1]. Experimental results for different extensions of the passive region together with preliminary numerical results have been reported in [14]. These showed that fluxon motion ceases to be stable when the ratio of the widths of the passive region and the junction becomes larger than 3. The influence of the electric parameters was not studied.

In a recent work one of the authors studied the case of a window junction with a homogeneous lateral passive region with periodic boundary conditions in the longitudinal direction. The motion of kinks in such a device occurs for velocities which can be calculated from the parameters of the device. In this study we will show that the presence of the passive region along the direction

of propagation will impose the velocity of the kink.

We have studied the problem in a systematic way by comparing the solution of an effective 1D problem with the 2D solution. We varied both the geometrical parameters and the electric parameters. In a first step we considered the propagation of a kink across an interface where the coefficient of the kink term and the electric properties vary abruptly. The operator describing this situation is discontinuous and one needs to use a finite volume approximation in order to have an accurate numerical solution. This method based on integrating the operator on reference volumes enables to satisfy exactly the jump conditions at the interface. Using this well suited numerical method together with soliton perturbation techniques, we have derived simple models explaining the dynamics of kinks in a window junction.

The paper is organized as follows, in section 2 we introduce the 2D partial differential equation model. In section 3 we obtain an effective 1D model for the case where the passive region exists only at each end of the junction. In section 4 we study kink motion across an interface, we derive the perturbation equations, analyze their fixed points and validate this approach by comparing the solution to the one given by a numerical integration of the partial differential equation. Section 5 discusses kink motion in a 1D and 2D window junction. In section 6 we present kink motion instabilities in the system, consider limiting cases and give our concluding remarks.

2 The model

The electrodynamics of a window junction can be described by two 2D arrays of inductances coupled together through an RSJ element containing a capacitor, the nonlinear Josephson element and a resistor[15,16]. This approach is equivalent to a discretisation of Maxwell's equations together with Josephson's constitutive equation. We then assume perfect symmetry and go to the continuum limit to obtain the following partial differential equation for the

evolution of the phase difference ϕ in a domain Ω

$$C\phi_{tt} - \operatorname{div}\left(\frac{1}{L}\nabla\phi\right) + \epsilon(x, y)(\sin(\phi) + \alpha\phi_t) = 0, \quad (1)$$

where C and L are respectively the normalized capacitance per unit surface and inductance and $\epsilon(x, y)$ is the indicator function of the junction domain Ω_J (ie $\epsilon = 1$ in Ω_J and 0 outside). The unit of space is the Josephson penetration depth and the unit of time the plasma frequency in the junction [3].

Defining C_I and L_I to be respectively the normalized capacitance per unit surface and inductance in the passive region, Equation (1) can be rewritten as the system

$$\frac{\partial^2\phi}{\partial t^2} - \Delta\phi + \sin\phi + \alpha\frac{\partial\phi}{\partial t} = 0 \quad \text{in } \Omega_J, \quad (2)$$

$$C_I\frac{\partial^2\psi}{\partial t^2} - \frac{1}{L_I}\Delta\psi = 0 \quad \text{in } \Omega \setminus \Omega_J, \quad (3)$$

together with the interface conditions for the phase and its normal gradient the surface current on the junction boundary $\partial\Omega_J$

$$\psi = \phi \quad \text{and} \quad \frac{1}{L_I}\frac{\partial\psi}{\partial n} = \frac{\partial\phi}{\partial n} \quad (4)$$

where n is for example the exterior normal. The boundary condition on the boundary of the passive region represents the input of an external current or magnetic field

$$\frac{1}{L_I}\frac{\partial\psi}{\partial n} = f. \quad (5)$$

Note that the jump condition (2nd relation in (4)) can be obtained by integrating (1) on a small surface overlapping the junction domain Ω_J .

In the rest of the paper we have assumed a rectangular window of length $l = 10$ and width $w = 1$ embedded in a rectangular passive region of extension w' as shown in Figure 1. We will not consider the influence of an external magnetic field and will assume the external current feed to be of overlap type so that the boundary conditions (5) become

$$\begin{aligned} \frac{1}{L_I} \frac{\partial \psi}{\partial y} &= \mp \frac{I}{2(l+2w')} \quad \text{for} \quad y = \pm \left(\frac{w}{2} + w'\right). \\ \frac{\partial \psi}{\partial x} &= 0 \quad \text{for} \quad x = \pm \left(\frac{l}{2} + w'\right). \end{aligned} \quad (6)$$

We assumed throughout the study a small damping $\alpha = 0.01$ which is typical of underdamped Josephson junctions.

3 The 1D effective model

In this section we introduce a simplified model where the passive region exists only on the longitudinal sides of the junction as in the bottom right panel of Fig. 1. Then the functions L and ϵ depend only on the variable x . To simplify the problem we assume a uniform boundary condition $\frac{\partial \psi}{\partial y} = \mp \frac{I}{2(l+2w')}$ for $y = \pm \left(\frac{w}{2} + w'\right)$.

We will show that this system is well described in the limit of a small current I by a one dimensional sine-Gordon equation.

For that we write the solution of (1) as $\phi = \phi_I + \phi_R$ where

$$\phi_I = -\frac{Iy^2}{2w(l+2w')} \quad (7)$$

satisfies the y boundary conditions. These also imply that the residual ϕ_R is even in y and can be expanded in a cosine Fourier series

$$\phi_R = \sum_{n=0}^{\infty} A_n(x, t) \cos \frac{2n\pi y}{w} . \quad (8)$$

Inserting (7) and (8) into (1) we obtain

$$\begin{aligned} C[A_{0tt} + A_{1tt} \cos \frac{2\pi y}{w} + \dots] - \left[\frac{1}{L} (A_{0x} + A_{1x} \cos \frac{2\pi y}{w} + \dots) \right]_x - \left[\frac{1}{L} \left(-\frac{Iy}{w(l+2w')} \right. \right. \\ \left. \left. - \frac{2\pi}{w} A_1 \sin \frac{2\pi y}{w} + \dots \right) \right]_y + \epsilon(x) [\sin(\phi_I + A_0 + A_1 \cos \frac{2\pi y}{w} + \dots) + \alpha(A_{0t} + A_{1t} \cos \frac{2\pi y}{w} + \dots)] = 0 . \end{aligned}$$

We get the evolution of A_0 by integrating the equation above in y and dividing by w ,

$$CA_{0tt} - \left(\frac{1}{L} A_{0x} \right)_x + \frac{I}{Lw(l+2w')} + \epsilon(x) \left[\frac{1}{w} \int_{\frac{-w}{2}}^{\frac{w}{2}} \sin(\phi_I + A_0 + A_1 \cos \frac{2\pi y}{w} + \dots) dy + \alpha A_{0t} \right] = 0 .$$

We write

$$\sin(\phi_I + A_0 + A_1 \cos \frac{2\pi y}{w} + \dots) \approx \sin(\phi_I + A_0) + A_1 \cos \frac{2\pi y}{w} \cos(\phi_I + A_0)$$

because $|A_1| \ll |A_0|$. First we consider the integral of the first term $\sin(\phi_I + A_0)$

$$\int_{\frac{-w}{2}}^{\frac{w}{2}} \sin(\phi_I + A_0) dy = \cos(A_0) \int_{\frac{-w}{2}}^{\frac{w}{2}} dy \sin(\phi_I) + \sin(A_0) \int_{\frac{-w}{2}}^{\frac{w}{2}} dy \cos(\phi_I)$$

The first integral on the right hand side can be written

$$\int_{\frac{-w}{2}}^{\frac{w}{2}} dy \sin(\phi_I) = w \int_0^1 d\zeta \sin\left(-\frac{Iw}{8(l+2w')} \zeta^2\right)$$

so that if $-\frac{Iw}{8(l+2w')} \ll 1$ the sine can be linearized and the cosine taken equal to 1 leading to

$$\int_{\frac{-w}{2}}^{\frac{w}{2}} \sin(\phi_I + A_0) dy = -\frac{Iw}{24(l+2w')} \cos(A_0) + w \sin(A_0) .$$

The terms in A_1 are

$$A_1 \cos(A_0) \int_{\frac{-w}{2}}^{\frac{w}{2}} dy \cos(\phi_I) \cos \frac{2\pi y}{w} - A_1 \sin(A_0) \int_{\frac{-w}{2}}^{\frac{w}{2}} dy \sin(\phi_I) \cos \frac{2\pi y}{w} .$$

Both terms can be treated following the same approximations as above so that

$$\int_{\frac{-w}{2}}^{\frac{w}{2}} dy \cos(\phi_I) \cos \frac{2\pi y}{w} \approx \frac{w}{\pi} ; \quad \int_{\frac{-w}{2}}^{\frac{w}{2}} dy \sin(\phi_I) \cos \frac{2\pi y}{w} = -\frac{Iw^2}{4\pi^3(l+2w')} .$$

Combining all contributions, we obtain for the evolution of A_0

$$CA_{0tt} - \left(\frac{1}{L} A_{0x} \right)_x + \frac{I}{Lw(l+2w')} + \epsilon(x)[\sin(A_0) - \frac{Iw}{24(l+2w')} \cos(A_0) + A_1 \left(\frac{w}{\pi} \cos(A_0) - \frac{Iw^2}{4\pi^3(l+2w')} \sin(A_0) \right) + \alpha A_{0t}] = 0. \quad (9)$$

For the values of the geometric parameters that we have taken $l = 10, w = 1, |w'| \leq 10$ and if we assume $I < 1$ which is the case for a zero field step then the terms $\frac{Iw}{24(l+2w')}, \frac{w}{\pi}, \frac{Iw^2}{4\pi^3(l+2w')}$ can be neglected so that we are left with the following sine-Gordon equation for A_0 (dropping the 0)

$$CA_{tt} - \left(\frac{1}{L} A_x \right)_x + \gamma(x) + \epsilon(x)[\sin(A) + \alpha A_t] = 0, \quad (10)$$

where $\gamma(x) = \frac{I}{L(x)w(l+2w')}$. This approach is validated for a homogeneous 2D sine-Gordon equation by the numerical evidence provided by Eilbeck and al [24] that when $(I/8\mathcal{L} \ll 1)$, the phase is almost uniform in the y direction.

4 Motion of a kink across a 1D interface

Before considering the motion of a kink in a window junction, we will study the simpler problem of an interface between two media with different values of the parameters $\{L(x), C(x), \epsilon\}$. The propagation of a soliton across an interface has been studied by many authors [19], [20], [21]. A pioneering work was done by Aceves et al [25] for the motion of a nonlinear Schrödinger soliton between two media of different Kerr indices. It was shown that the soliton perturbation equations give a qualitatively correct description even when the nonlinearity of the second medium is very small. We will follow the same route and derive adiabatic equations for the soliton parameters. These are in principle only valid for small perturbations but some ideas can be obtained by taking the limit $\epsilon \rightarrow 0$. In this way one can understand qualitatively the motion of a kink from a junction to a passive region.

Following [19], we introduce the change of variable

$$dz = \sqrt{L(x)}dx, \quad (11)$$

which makes the perturbation theory regular in the sense that the solution has the same form on the left and right of the interface. In principle the terms CA_{tt} and $\epsilon \sin A$ make the perturbation theory singular, however we are mostly interested in the fixed points that exist due to the interfaces, The first term will not influence these, nor their stability. We expect this description to hold if the wave remains close to the interface.

Then we write equation (10) in standard form

$$A_{tt} - A_{zz} + \sin(A) = -\gamma(x) - \alpha A_t + (1 - \epsilon(x)) \sin(A) + (1 - C(x)) A_{tt} - \frac{1}{2} \partial_z [\ln L(x)] A_z. \quad (12)$$

To simplify the calculations we assumed a uniform damping α . To model the experimental situation of [14] for example, it is natural to assume the following dependencies for the parameters L , C and ϵ

$$L(x) = \begin{cases} 1 & \text{if } x < 0 \\ L_I & \text{if } x > 0 \end{cases}, \quad C(x) = \begin{cases} 1 & \text{if } x < 0 \\ C_I & \text{if } x > 0 \end{cases} \quad \text{and} \quad \epsilon(x) = \begin{cases} 1 & \text{if } x < 0 \\ \epsilon_0 & \text{if } x > 0 \end{cases}.$$

With this type of distribution of the inductance L and using (11) we obtain the differential relation $\partial_z [\ln L(x)] = (\ln(L_I))\delta(z)$, where δ is the Dirac delta function.

Now we rearrange the right hand side of Eq. (12) as the perturbation term

$$\epsilon f = -\gamma_J - \alpha A_t + [-(\gamma_I - \gamma_J) - \mu_0 \sin A + (1 - C_I) A_{tt}] H(z) - \frac{\ln(L_I)}{2} \delta(z) A_z, \quad (13)$$

where $\mu_0 = \epsilon_0 - 1$, $\gamma_I = \frac{I}{L_I w(l+2w')}$, $\gamma_J = \frac{I}{w(l+2w')}$ and H is usual Heaviside function.

Note that the functions C and ϵ are piece-wise constants and therefore there is no different re-scaling on each side of the interface as we go from the variable x to z . Having set up the problem (12), we assume as usual that the soliton parameters are slowly modulated and use perturbation theory [22] to derive their evolution.

We choose the kink ansatz

$$A_a(z, t) = 4 \tan^{-1} \exp \sigma \left(\frac{z - Z(t)}{\sqrt{1 - v^2}} \right),$$

where $Z(t) = \int_0^t v(t') dt' + z_0(t)$ and $\sigma = 1$ (resp. -1) for a kink (resp. antikink).

Then $(Z(t), v(t))$ are solutions of the differential system

$$\begin{aligned} \frac{dZ}{dt} &= v - \frac{\mu_0 v(1 - v^2)}{2} \left(1 + \tanh \left(\frac{Z}{\sqrt{1 - v^2}} \right) \right) - \frac{Zv}{\sqrt{1 - v^2}} \left(\frac{\mu_0(1 - v^2)}{2} + \frac{\ln(L_I)}{4} \right) \\ &\quad \times \operatorname{sech}^2 \left(\frac{Z}{\sqrt{1 - v^2}} \right) + \frac{(1 - C_I)v^2\sqrt{1 - v^2}}{4} \left(1 - \frac{Z}{\sqrt{1 - v^2}} \right) \left[1 + \tanh \left(\frac{Z}{\sqrt{1 - v^2}} \right) \right] \\ &\quad - \frac{v}{4}(\gamma_I - \gamma_J)\sqrt{1 - v^2}2G, \end{aligned} \quad (14)$$

$$\begin{aligned} \frac{dv}{dt} &= \frac{\pi\sigma(\gamma_I + \gamma_J)(1 - v^2)^{\frac{3}{2}}}{8} - \alpha v(1 - v^2) - \frac{\sqrt{1 - v^2}}{4} \left(\mu_0(1 - v^2) - \ln(L_I) \right) \\ &\quad \times \operatorname{sech}^2 \left(\frac{Z}{\sqrt{1 - v^2}} \right) + \frac{(1 - C_I)v^2\sqrt{1 - v^2}}{4} \operatorname{sech}^2 \left(\frac{Z}{\sqrt{1 - v^2}} \right), \end{aligned} \quad (15)$$

where $2G = 1.831931188..$ [23]. If we assume $\epsilon \equiv 1$, $\alpha = I = 0$ and $C_I = 1$ these equations are exactly the ones derived in [19].

In the absence of the current and the damping, the equations (14-15) derive from the Hamiltonian,

$$H = \int_{-\infty}^{+\infty} L(z)^{-1/2} \left[\frac{C(z)}{2} \left(\frac{\partial \varphi}{\partial t} \right)^2 + \frac{1}{2} \left(\frac{\partial \varphi}{\partial z} \right)^2 + \epsilon(z)(1 - \cos \varphi) \right] dz. \quad (16)$$

If we assume the fluxon to have velocity v_l for $z \ll 0$, its energy is $H_l(v_l) = \frac{8}{(1 - v_l^2)^{1/2}}$. If it crosses into the passive medium $z \gg 0$, it will have a velocity v_r and energy $H_r(v_r)$

$$H_r(v_r) = \frac{4v_r^2(C_I - \epsilon_0) + 4(1 + \epsilon_0)}{L_I^{1/2}(1 - v_r^2)^{1/2}}, \quad (17)$$

and one can obtain the condition on the velocity v_l so that the left coming soliton crosses into the right hand medium as $H_l(v_l) \geq H_r(v_r = 0)$ which

implies $v_l^2 > 1 - \frac{4L_I}{(1+\epsilon_0)^2}$. One can then compute v_r by identifying H_l and H_r . If $v_l < \sqrt{1 - \frac{4L_I}{(1+\epsilon_0)^2}}$ the fluxon is reflected with velocity $-v_l$.

4.1 Existence and stability of fixed points

From the above equations, we obtain two fixed points symmetrically placed with respect to the interface $z = 0$

$$Z_{\pm} = \operatorname{atanh} \eta_{\pm} \equiv \operatorname{atanh} \left(\pm \sqrt{1 + \frac{\pi\gamma\sigma}{\epsilon_0 - 1 - \log(L_I)}} \right)^{\frac{1}{2}}, \quad (18)$$

where $\gamma = \frac{(\gamma_I + \gamma_J)}{2}$.

The expression indicates that at least two ingredients are necessary for soliton trapping at a finite distance from the interface, a DC current γ , a jump in the coefficient of the sine nonlinearity ϵ (the critical current density in the Josephson model) and an inductance jump L_I . Trapping has been predicted with the first two features in the works [20,21]. Notice also that the existence and position of the fixed points is completely independent of the damping α and capacity C_I in the passive region.

Let us consider the conditions for existence of these fixed points. For that we separate the cases of a kink or an antikink. For a kink $\sigma = 1$, the fixed points exist if $\mu_0 - \log(L_I) - \pi\gamma \geq 0$ or $L_I \leq e^{\mu_0 - \pi\gamma}$ while for the antikink $\sigma = -1$ they exist if $L_I \geq e^{\mu_0 + \pi\gamma}$.

To investigate the stability of these fixed points we compute the Jacobian of the evolution equations (14-15) and estimate its eigenvalues λ at each of the fixed points. The characteristic equation is

$$\lambda^2 + \lambda\alpha - \frac{\pi\gamma\sigma\eta_{\pm}}{2} \left[1 - \frac{\mu_0}{2} (1 + \eta_{\pm}) - \frac{\pi}{2} Z_{\pm} \gamma \sigma \frac{\mu_0 + \frac{\log(L_I)}{2}}{\mu_0 - \log L_I} \right] = 0.$$

Let us fix the type of wave to be an antikink. Then we find that the discriminant for the fixed point Z_+ is negative for any value of the current and tends to zero as the current tends to zero. This fixed point is then stable because

Fig. 1. Table 1: existence and stability of the fixed points Z_{\pm}

	$L_I \leq e^{\epsilon_0 - 1 - \pi\gamma}$	$e^{\epsilon_0 - 1 - \pi\gamma} \leq L_I \leq e^{\epsilon_0 - 1 + \pi\gamma}$	$e^{\epsilon_0 - 1 + \pi\gamma} \leq L_I$
antikink ($\sigma = -1$)	no fixed points	no fixed points	2 fixed points Z_{\pm} Z_+ is stable Z_- is unstable
kink ($\sigma = 1$)	2 fixed points Z_{\pm} Z_+ is unstable Z_- is stable	no fixed points	no fixed points

the eigenvalues are complex conjugate and their real part $-\alpha/2$ is negative.

On the other hand the fixed point Z_- is unstable because the discriminant is always positive and the eigenvalues are of opposite signs.

If we had considered as for the 2D problem that dissipation is absent on the right hand medium, we would have obtained half the damping term in the equation for dv/dt and an additional term $\alpha \frac{\epsilon}{2} \sqrt{1 - v^2} v^2 \sigma \log(2)$ in the equation for dZ/dt . The first term would affect the stability, it is equivalent to halving the overall damping term.

The existence and stability for both kink and antikink waves is summarized in Table 1.

This study that such an interface enables to trap a certain type of wave. For large L_I , antikinks are trapped at a fixed point $X_+ = Z_+/\sqrt(L_I)$ in the passive region while kinks remain free. On the contrary when L_I is small, kinks are trapped at the fixed point $X_- = Z_-$. If the interface is now such that the passive region is for $z < 0$ and the junction for $z > 0$, then the second column and the last column of the table should be permuted and the stability properties exchanged. This provides a qualitative understanding of the window device which contains two such interfaces.

4.2 Validation of the perturbation theory

In order to test these predictions we have compared the solution of the partial differential equation (10) with the solution of the perturbation equations (14-15). Note that the former is a generalized operator with discontinuities in the coefficients so that the solution is continuous but exhibits jumps of its derivative at the junction interface. To obtain it we introduce the finite volume method used for the treatment of hyperbolic equations [26]. The idea is to integrate the partial differential equation over intervals around each discretisation point where the solution is assumed constant. In this way the jump conditions are exactly respected. The details of the implementation for both the 1D and 2D cases are given respectively in appendices A and B.

Fig. 2 shows the phase plane in the original position-velocity coordinates (X, u) for an antikink wave for two different interfaces with $\epsilon_0 = 0.6, \gamma = 0.02$ and $L_I = 1$ (top panel) and $L_I = 1.5$ (bottom panel). The solution of the perturbation equations is given in full line while the solution of the partial differential equation is given by the crosses. A least square procedure has been used to estimate the position and velocity of the wave. For both cases we obtain a good overall agreement between the solution of the partial differential equation and the perturbation approach, showing that the fixed point traps the antikink even for a large initial velocity ($u = 0.5$). For the bottom panel where $L_I = 1.5$ notice the jump in the phase gradient and the fact that the fixed point is close to the interface as expected.

We now consider that the nonlinear term on the right hand side is very small. Fig. 3 shows $X(t)$ and $u(t)$ for an antikink in the case $L_I = 1$ and $\epsilon_0 = 0.1$. For such a strong perturbation, we obtain a qualitative agreement for both the position and velocity of the wave between the solutions of (10) and (14-15). Both the numerical solution and the perturbation method show the existence of a stable fixed point located in the region $\epsilon(x) = \epsilon_0 < 1$. We therefore expect (14-15) to provide qualitative results even for $\epsilon_0 \rightarrow 0$ i.e. the nonlinear-linear interface. It is then possible to use these arguments to describe the motion of a kink in a window junction where the passive region exists on both sides of

the Josephson junction.

5 Motion of a kink in a window junction

5.1 The perturbation theory

As shown in the perturbation equations (14-15) the motion of a kink is due to the injection of direct current in the device, described by the γ term. In a pure Josephson junction, this gives rise to the well-known Zero (magnetic) Field Steps in the current voltage IV characteristics. The presence of passive regions where no sine term is present and for which there is an inductance jump will affect the kink motion. We will concentrate in this study on the features of this motion. The study of the IV characteristics and its associated zero field step will be presented in [17].

The study conducted above for the case of a single interface provides a way to give a simple description of the fluxon motion in a one dimensional window junction (bottom left panel in Fig. 1). In that case the current density is $\gamma_{1dw} = I(1 + 1/L_I)/(2(l + 2w'))$ and the position of the fixed points is

$$X_{\pm} = \frac{1}{L_I} \operatorname{atanh} \left(\pm \left(1 + \frac{\pi\gamma\sigma}{\epsilon_0 - 1 - \log(L_I)} \right)^{\frac{1}{2}} \right), \quad (19)$$

This quantity depends weakly on both the current I and the inductance in the passive region L_I . For the parameters used here $\epsilon_0 = 0$, $l = 10$, the fixed point is inside the domain as soon as $w' \geq 2$.

Fig. 4 shows the schematic motion of a wave in such a device, in the limiting cases $L_I \gg 1$ (top panel) and $L_I \ll 1$ (bottom panel). The antikink wave propagates towards the right and gets reflected as a kink at the right boundary of the device. When $L_I \gg 1$, the antikink finds two fixed points on each side of the interface, identified by large or small circles depending whether the fixed point is stable or unstable. The antikink is slowed down and can be trapped at the fixed point located to the left of the left interface. The kink can become

trapped at the fixed point of the right interface. The situation is reversed for $L_I \ll 1$. We see that these points will affect the motion and could hinder wave motion.

5.2 Numerical study

To confirm the role of the fixed points at the interfaces we carried out a systematic study of the kink motion in both a 1D and a 2D configuration. The numerical procedure in both cases is to discretize the spatial operator using the finite volume approximation which allows to preserve the interface conditions (see Appendix A and B). The temporal part is then advanced using the Dormand and Prince ordinary differential equation solver DOPRI5 implemented by Hairer and Norsett [27]. The initial condition is a static kink for the 1D junction and the static solution [7] in the case of a 2D window junction. The wave is then accelerated by the injection of direct current through the boundary conditions (6). It will reach its limiting velocity which can be obtained by simple arguments.

Figure 5 presents the motion of a kink at its limiting velocity in a 1D window junction. The top and middle panels show respectively the position $X(t)$ and velocity $u(t)$ vs. time while the bottom panel shows the phase plane (X, u) . The electric parameters are $L_I = C_I = 2$ so that the velocity of the linear waves in the passive region is $v_I = 1/\sqrt{L_I C_I} = 0.5$. One sees that the kink velocity is close to 1 in the junction region while it is about 0.5 in the passive region, so the kink adapts its speed to the region it travels in. At this point it is interesting to remark that the kink continues to exist even in the regions where there is no sine term. The whole motion and the voltage observed are then given by the expression

$$V_{1D} \equiv \langle \phi_t \rangle = \frac{\Delta\phi}{\Delta t} = \frac{2\pi}{2w'/v_I + l}. \quad (20)$$

The motion of a kink in a 2D window junction is different as can be seen from Figure 6 which shows a contour plot of the phase $\varphi(x, y, t)$ for 4 successive values of time. The parameters are the same as in Figure 5. In this case

no significant change is observed in the speed of the wave in the junction and passive regions. The voltage observed indicates that the velocity is everywhere equal to the one in the passive region $v_I = 1/\sqrt{L_I C_I}$. There is a simple explanation for this, the soliton velocity is a free parameter for the sine Gordon equation. In the linear region waves can only travel at velocity v_I . The dressed kink which carries a significant part of its energy in the passive region adapts its speed to v_I . The voltage in this case is

$$V_{2D} = \frac{2\pi v_I}{2w' + l}. \quad (21)$$

For a large extension w' of the passive region or values of the electric parameters non equal to 1, the kink motion can break down. In the next section, we give a few examples of this phenomenon.

6 Instabilities and limiting cases

In our procedure, we take as initial condition a static kink and accelerate it by injecting current via the boundary condition (5). We present now a few situations where this procedure led to the break down of the kink and another type of dynamical behavior occurred. The situation is simpler for the 1D window junction and we will present this first.

In the 1D case, the kink (antikink) can be trapped at the fixed point on the right (left) end interface. This occurs because as the width of the passive region w' is increased, the current density is decreased so that there is less driving force to overcome the potential barrier created by the stable fixed point. For the junction geometry that we chose $l = 10, w = 1$ kink motion breakdown occurs for $w' \approx 10$.

The electrical parameters act differently. To see this consider the equations of the problem

$$\frac{\partial^2 \phi}{\partial t^2} - \frac{\partial^2 \phi}{\partial x^2} + \sin \phi + \gamma + \alpha \frac{\partial \phi}{\partial t} = 0 \quad |x| \leq \frac{l}{2}, \quad (22)$$

$$C_I \frac{\partial^2 \psi}{\partial t^2} - \frac{1}{L_I} \frac{\partial^2 \psi}{\partial x^2} + \gamma = 0 \quad \frac{l}{2} \leq |x| \leq \frac{l}{2} + w' , \quad (23)$$

together with the interface condition at $|x| = \frac{l}{2}$

$$\phi = \psi \quad , \quad \frac{1}{L_I} \frac{\partial \psi}{\partial x} = \frac{\partial \phi}{\partial x} \quad ,$$

and homogeneous boundary conditions $\frac{\partial \psi}{\partial x}|_{x=\pm(l/2+w')} = 0$.

When C_I or L_I are large we can consider their inverse as a small parameter and use perturbation theory to get some estimates. Let us first consider the case $C_I \gg 1$. Then from equation (23) we get $\frac{\partial^2 \psi}{\partial t^2} = 0$ so that $\frac{\partial \psi}{\partial t} = V$ is a constant. We then write $\psi = Vt + f(x)$ so that the (23) becomes

$$-\frac{d^2 f}{dx^2} + \gamma L_I = 0 ,$$

which yields $\frac{df}{dx} = \gamma L_I (x - l/2 - w')$ for $l/2 \leq x \leq l/2 + w'$ and $\psi = \gamma L_I (x - l/2 - w')^2/2 + Vt + Cte$. This fixes the boundary conditions for the first equation. When L_I is large $\frac{\partial \phi}{\partial x}|_{x=\pm l/2} \rightarrow 0$ so that kink motion is possible. On the contrary, kink motion becomes impossible when $L_I \ll 1$ because then $\frac{\partial \phi}{\partial x}|_{x=\pm l/2} \rightarrow \infty$.

Let us now consider the two dimensional situation. For large passive regions the static kink solution becomes stretched and occupies the whole junction [1]. It is then difficult to accelerate and generally it breaks up after a few round trips. Figure 7 shows contour plots of the phase $\varphi(x, y, t)$, numerical solution of (1) for $t = 0, 5, 6$ and 8 clockwise starting from the top left panel, for a large passive width $w' = 7$. One sees that the kink breaks up and leads to a radial phase distribution centered on the junction. The wave equation then dominates the dynamics and the average phase increases with time.

Another type of instability is due to the electrical parameters L_I and C_I , especially the former because it acts on the interface condition in addition to the operator. For example consider $L_I = 10^{-4}$ and $w' = 2$, the case of Figure 8 where the phase $\varphi(x, y, t)$ is shown for $t = 2, 10$ and 20 from left to right. The top panels show the contours while the bottom ones show the three dimensional plots. The phase tends to obey a Laplace equation in the passive

region and there the kink leads to a uniform phase distribution. The junction is strongly coupled to the passive region because the gradient at the interface is very large. This causes the break-up of the initial kink and leads to a radial solution with small oscillations.

A very large inductance leads to the creation of a boundary layer along the top and bottom edges of the device as shown in Figure 9 which presents two snapshots for successive times. In this case $L_I = 10^4$. At the interface the gradient of φ is close to zero, so that the phase is constant in the junction. Notice the strong gradients on the top and bottom sides of the passive region.

For $w' = 2$, we have found in the (L_I, C_I) plane, the region of instability of the kink as shown in Figure 10. We plotted in the (L_I, C_I) plane, the hyperbolas corresponding to three values of velocity in the passive region, $v_I = 0.5, 1$ and 2 . The signs $(*)$ (\times) and $(+)$ indicate where we found a stable kink motion. We have isolated by the solid curve the stability region in the (L_I, C_I) plane. As expected the instability is due essentially to the inductance L_I so the kink is stable in the domain $0.1 \leq L_I \leq 2$. In this interval we always observed kink motion independently of the value of the capacity C_I . For example for a capacity $C_I = 10^4$ and $L_I = 1$, we obtain a stable kink motion. The voltage observed $V_{\text{num}} 2D = 4.510 \times 10^{-3}$ is in good agreement with the one given by (21), $V_{2D} = 4.5 \times 10^{-3}$. Then we conclude that the region of stability of the kink in the window problem is

$$D_{\text{stability}} = \{0.1 \leq L_I \leq 2\}. \quad (24)$$

At this time we do not have an explanation for this threshold value $L_I = 2$.

From a general point of view this study has shown the importance of the perturbation approach to gain insight into a complicated wave problem. Another determining factor was the use of the finite volume discretisation to solve the inhomogeneous partial differential equation.

Acknowledgments

The Authors thank A. C. Scott, A. Ustinov, and S. Flach for helpful discus-

sions. A. B. thank the department of Mathématiques de l'INSA de Rouen. J. G. C. thank the Max Planck institute for the Physics of complex systems, Dresden, for its hospitality during a short visit. This work was supported by the European Union under the RTN project LOCNET HPRNCT-1999-00163.

References

- [1] J. G. Caputo, N. Flytzanis et M. Devoret, *Phys. Rev. B* **50** (1994) 6471.
- [2] J. G. Caputo, N. Flytzanis et M. Vavalis, *Int. J. Mod. Phys. C* **6** (1995) 241.
- [3] A. Barone and G. Paterno, *Physics and Applications of the Josephson effect*, J. Wiley, (1982).
- [4] J. Frenkel and T. R. Kontorova, *J. Phys. Soviet Union* 1, (1939), 137
- [5] R. K. Dodd, J. C. Eilbeck, J. D. Gibbon and H. C. Morris, *Solitons and nonlinear wave equations*, Academic Press, (1984).
- [6] M. Remoissenet, J. M. Tamga and J. Pouget, in *Nonlinear coherent structures in physics and biology*, K. H. Spatschek and F. G. Mertens Eds., Plenum press, (1994).
- [7] J. G. Caputo, N. Flytzanis and M. Vavalis, *Int. J. Mod. Phys. C* **7** (1996) 191.
- [8] J. G. Caputo, N. Flytzanis, V. Kurin, N. Lazarides and M. Vavalis, *J. Appl. Phys.* **85** (1999) 7291.
- [9] A. Ustinov et al, submitted to *J. Appl. Physics*, April 2000.
- [10] G. S. Lee, *I.E.E.E. Trans. Appl. Superconductivity*, **1** (1991) 121.
- [11] G. S. Lee and A. T. Barfknecht, *I.E.E.E. Trans. Appl. Superconductivity*, **2** (1992) 67.
- [12] R. Monaco, G. Costabile and N. Martucciello, *J. Appl. Phys.* **77** (1995) 2073.
- [13] Nonlinear superconducting devices and hight T_c materials, R. D. Parmentier and N. F. Pedersen (Eds.), World Scientific, (1995).
- [14] N. Thyssen et al, in [13].

- [15] M. Devoret, private communication.
- [16] K. K. Likharev, "Dynamics of Josephson junctions and circuits", Gordon and Breach, (1986).
- [17] A. Benabdallah and J. G. Caputo, Influence of the passive region on zero field steps for window Josephson junctions, submitted to J. Appl. Phys.
- [18] A. Benabdallah, Doctoral thesis, University of Rouen, May 1999.
- [19] S. Sakai, M. R. Samuelsen and O. H. Olsen, Phys. Rev. B **36** (1997) 217.
- [20] Y. Kivshar and B. Malomed, *J. Appl. Phys.* **65** (1989) 879.
- [21] Y. Kivshar and O. Chubykalo, *Phys. Rev. B* **43** (1991) 5419.
- [22] D.W. McLaughlin and A.C.Scott, *Phys. Rev. A* **18** (1978) 1652.
- [23] I. S. Gradshteyn and I. M. Ryzhik *Tables of Integrals, Series and Products* Academic Press., N.Y. (1994).
- [24] J. C. Eilbeck, P. S. Lomdahl, O. H. Olsen and M. R. Samuelsen, *J. Appl. Phys.* **57** (1985) 861.
- [25] A. B. Aceves, J. V. Moloney , and A. C. Newell, *Phys. Rev. A* **39** (1989) 1809.
- [26] *Finite volumes for complex applications II: problems and perspectives*, R. Vilsmeier, F. Benkhaldoun and D. Hanel Eds., Hermès, (1999).
- [27] E. Hairer, S. P. Norsett and G. Wanner, Solving ordinary differential equations I, Springer-Verlag (1987).

APPENDIX A: The finite volume formulation in 1D

We introduce new functions for the 1D window equation (10)

$$u = A_t \quad \text{and} \quad v = A_x ,$$

which becomes the system

$$\frac{\partial U}{\partial t} + \frac{\partial (\mathcal{A}U)}{\partial x} = \mathcal{B}(U, A) , \quad (25)$$

where

$$U = \begin{bmatrix} u \\ v \end{bmatrix}, \quad \mathcal{A}(x) = \begin{bmatrix} 0 & -\frac{1}{L(x)C(x)} \\ -1 & 0 \end{bmatrix},$$

and

$$\mathcal{B}(U, A) = \begin{bmatrix} -\frac{\epsilon(x)}{C(x)}(\alpha u + \sin A) - \frac{\gamma}{C(x)} - \frac{\partial}{\partial x} \left(\frac{1}{C(x)} \right) \frac{1}{L(x)} v \\ u \end{bmatrix}.$$

The matrix \mathcal{A} has two real eigenvalues $\lambda_{1,2} = \pm \sqrt{\frac{1}{L(x)C(x)}}$ thus the system (25) is strictly hyperbolic with a source term. Due to the discontinuities of the functions $C(x)$, $L(x)$ and $\epsilon(x)$ at the interfaces, the numerical integration of the Eq. (25) using finite differences cannot be done. We therefore turn to the finite volume method [26], whose principle is first to consider a partition of the passive and junction domain in cells

$$V_k^{i,j} = \left\{ x \mid x_k - \frac{h_{i,j}}{2} \leq x < x_k + \frac{h_{i,j}}{2} \right\},$$

where x_k are collocation points defined by

$$\begin{aligned} x_k &= (k - \frac{1}{2})h_i \text{ in passive region ,} \\ x_k &= (k - 1)h_j \text{ in junction region .} \end{aligned}$$

Here h_i and h_j are the space mesh-length, defined by

$$h_i = \frac{w'}{n_i + \frac{1}{2}}, \quad h_j = \frac{l}{n_j - 1},$$

where n_i and n_j respectively are the number of discretization in the passive and junction domain. The total number points of the whole domain is $2n_i + n_j$. Notice that the points x_k such $k = n_i$ and $k = n_i + n_j$ correspond to the real interface points $x = -l/2$ and $x = l/2$.

In a second step we assume the solution of Eq. (25) to be constant in each cell $V_k^{i,j}$. We integrate Eq. (25) over each cell

$$\int_{V_k^{i,j}} \frac{\partial U}{\partial t} + \frac{\partial(\mathcal{A}U)}{\partial x} dx = \int_{V_k^{i,j}} \mathcal{B} dx, \quad (26)$$

and obtain

$$\mu(V_k^{i,j}) \frac{dU_k}{dt} + [\mathcal{A}U]_{\partial V_k^{i,j}} = \int_{V_k^{i,j}} \mathcal{B}(U, A) \, dx + \mathcal{O}(h^2) ,$$

where $U_k = U(x)$ for all $x \in V_k^{i,j}$.

We therefore obtain the following system of ordinary differential equations **In the passive region**

$$\frac{d}{dt} \begin{bmatrix} u_k \\ v_k \end{bmatrix} = \begin{bmatrix} \frac{1}{L_I C_I h_i} (v_h(x_k + \frac{h_i}{2}) - v_h(x_k - \frac{h_i}{2})) \\ -\frac{u_h(x_k + \frac{h_i}{2}) - u_h(x_k - \frac{h_i}{2})}{h_i} \end{bmatrix} - \begin{bmatrix} \frac{\gamma}{C_I} \\ 0 \end{bmatrix} , \quad (27)$$

which in terms of A yields

$$\left\{ \begin{array}{l} \frac{dA_k}{dt} = u_k \\ \frac{du_k}{dt} = -\frac{\gamma}{C_I} + \frac{A_{k+1} - 2A_k + A_{k-1}}{L_I C_I h_i^2} . \end{array} \right. \quad (28)$$

In the junction domain we obtain

$$\frac{\partial}{\partial t} \begin{bmatrix} u_k \\ v_k \end{bmatrix} = \begin{bmatrix} \frac{1}{h_j} (v_h(x_k + \frac{h_j}{2}) - v_h(x_k - \frac{h_j}{2})) \\ -\frac{u_h(x_k + \frac{h_j}{2}) - u_h(x_k - \frac{h_j}{2})}{h_j} \end{bmatrix} - \begin{bmatrix} \sin \varphi_k + \alpha u_k + \gamma \\ 0 \end{bmatrix} , \quad (29)$$

which in terms of A implies

$$\left\{ \begin{array}{l} \frac{dA_k}{dt} = u_k \\ \frac{du_k}{dt} = -\alpha u_k - \sin A_k - \gamma + \frac{A_{k+1} - 2A_k + A_{k-1}}{h_j^2} . \end{array} \right. \quad (30)$$

At the interface we get

$$\left\{ \begin{array}{l} \frac{h_i}{2} \begin{bmatrix} C_I & 0 \\ 0 & 1 \end{bmatrix} + \frac{h_j}{2} \begin{bmatrix} 1 & 0 \\ 0 & 1 \end{bmatrix} \end{array} \right\} \frac{\partial}{\partial t} \begin{bmatrix} u_k \\ v_k \end{bmatrix} = - \begin{bmatrix} 0 & L_I^{-1} \\ 1 & 0 \end{bmatrix} \begin{bmatrix} u_h \left(x_k + \frac{h_j}{2} \right) \\ v_h \left(x_k + \frac{h_j}{2} \right) \end{bmatrix} - \begin{bmatrix} 0 & 1 \\ 1 & 0 \end{bmatrix} \begin{bmatrix} u_h \left(x_k - \frac{h_i}{2} \right) \\ v_h \left(x_k - \frac{h_i}{2} \right) \end{bmatrix} - \begin{bmatrix} \frac{\gamma}{2} (h_i + h_j) + \frac{h_i}{2} (\alpha u_k + \sin A_k) \\ 0 \end{bmatrix}. \quad (31)$$

which in terms of A yields

$$\left\{ \begin{array}{l} \frac{dA_k}{dt} = u_k \\ \frac{du_k}{dt} = \frac{1}{C_I \frac{h_i}{2} + \frac{h_j}{2}} \left(\frac{A_{k+1} - A_k}{h_j} - \frac{A_k - A_{k-1}}{L_I h_i} - \frac{h_j}{2} (\alpha u_k + \sin A_k) - \gamma \left(\frac{h_i + h_j}{2} \right) \right) \end{array} \right. . \quad (32)$$

APPENDIX B: The finite volume formulation in 2D

Here we follow a similar procedure as in the 1D case. The discretization of the domain in the x direction is the same as done in the appendix A and in y direction we introduce the following partition

$$W_k^{i,j} = \left\{ y \mid y_k - \frac{h'_{i,j}}{2} \leq y < y_k + \frac{h'_{i,j}}{2} \right\},$$

where y_k are the collocation points defined by

$$\begin{aligned} y_k &= (k - \frac{1}{2})h'_i \text{ in passive region ,} \\ y_k &= (k - 1)h'_j \text{ in junction region .} \end{aligned}$$

Here h'_i and h'_j are the space mesh-length along y direction, defined by

$$h'_i = \frac{w'}{n'_i + \frac{1}{2}}, \quad h'_j = \frac{w}{n'_j - 1},$$

where n'_i and n'_j respectively are the number of discretization points in the passive and junction domains. The total number points in the whole domain is $(2n_i + n_j) \times (2n'_i + n'_j)$.

For convenience we choose the same step size in the whole domain (the number of points n_i, n_j, n'_i, n'_j are chosen such $h_i = h_j = h'_i = h'_j = h$). Then the discretization of the domain can be written as

$$\Omega = \bigcup_{k,k'} \Omega_{k,k'} ,$$

where

$$\Omega_{k,k'} = \left\{ (x, y) \mid x_k - \frac{h}{2} < x < x_k + \frac{h}{2} \text{ and } y_{k'} - \frac{h}{2} < y < y_{k'} + \frac{h}{2} \right\} ,$$

are squares of side lenght h centered at the point $(x_k, y_{k'})$.

We integrate equation (1) on each cell $\Omega_{k,k'}$ and use the finite volume approximation to obtain

$$\psi_{k,k'} \int_{\Omega_{k,k'}} C \, dx \, dy - \int_{\partial\Omega_{k,k'}} \frac{1}{L} \nabla \phi \cdot \mathbf{n} \, d\sigma + (\alpha \psi_{k,k'} + \sin(\phi_{k,k'})) \int_{\Omega_{k,k'}} \epsilon \, dx \, dy = 0 , \quad (33)$$

where $\psi = \dot{\phi}$, \mathbf{n} is the unit exterior normal to $\partial\Omega_{k,k'}$ and $\phi_{k,k'} = \phi(x, y)$, $\psi_{k,k'} = \phi_t(x, y)$ are assumed constant for all $(x, y) \in \Omega_{k,k'}$. We then obtain **for a cell inside the junction**

$$\begin{cases} \dot{\phi}_{k,k'} = \psi_{k,k'} \\ \dot{\psi}_{k,k'} = \frac{1}{h^2} [\phi_{k+1,k'} + \phi_{k,k'+1} + \phi_{k-1,k'} + \phi_{k,k'-1} - 4\phi_{k,k'}] + \sin \phi_{k,k'} + \alpha \psi_{k,k'} . \end{cases} \quad (34)$$

In the system defined above M, M' respectively are the total number of points in the x and y directions. For $k = 1, M$ and $k' = 1, M'$, the solution $(\phi_{k,k'}, \psi_{k,k'})$ is determined using the boundary condition (6).

For a cell in the passive region we obtain

$$\begin{cases} \dot{\phi}_{k,k'} = \psi_{k,k'} \\ \dot{\psi}_{k,k'} = \frac{1}{h^2 L_I C_I} (\phi_{k+1,k'} + \phi_{k,k'+1} + \phi_{k,k'-1} - 4\phi_{k,k'}) . \end{cases}$$

Now consider cells that are overlapping the interface. We will display two cases to show how the method works. First consider **the cell overlapping the bottom left corner of the junction boundary** ($x_k = -l/2, y'_k = -w/2$). There (33) yields

$$\begin{cases} \dot{\phi}_{k,k'} = \psi_{k,k'} \\ \dot{\psi}_{k,k'} = \frac{4}{h^2(3C_I+1)} [\phi_{k+1,k'} \frac{1}{2}(\frac{1}{L_I} + 1) + \phi_{k,k'+1} \frac{1}{2}(\frac{1}{L_I} + 1) + \phi_{k-1,k'} \frac{1}{L_I} \\ \quad + \phi_{k,k'-1} \frac{1}{L_I} - \phi_{k,k'}(1 + \frac{3}{L_I})] + \frac{1}{1+3C_I} (\sin \phi_{k,k'} + \alpha \psi_{k,k'}). \end{cases}$$

Second consider **a cell that is overlapping on the bottom boundary of the junction** ($-l/2 < x_k < l/2, y'_k = -w/2$). In that case we obtain

$$\begin{cases} \dot{\phi}_{k,k'} = \psi_{k,k'} \\ \dot{\psi}_{k,k'} = \frac{2}{h^2(C_I+1)} [\phi_{k+1,k'} \frac{1}{2}(\frac{1}{L_I} + 1) + \phi_{k,k'+1} + \phi_{k-1,k'} \\ \quad + \phi_{k,k'-1} \frac{1}{L_I} - \phi_{k,k'}(2 + \frac{2}{L_I})] + \frac{1}{1+C_I} (\sin \phi_{k,k'} + \alpha \psi_{k,k'}). \end{cases}$$

With this formulation we have checked the conservation of energy in the absence of current or damping $\alpha = I = 0$

$$E = \int_{\Omega} \left[\frac{C}{2} \left(\frac{\partial \psi}{\partial t} \right)^2 + \frac{1}{2L} |\nabla \psi|^2 + (1 - \cos(\phi)) \right] dx dy .$$

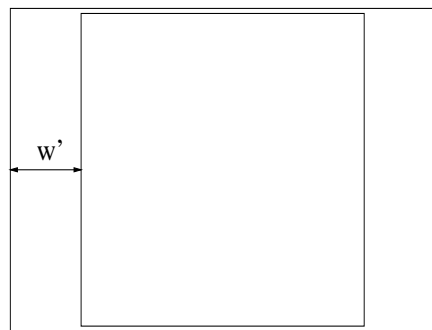
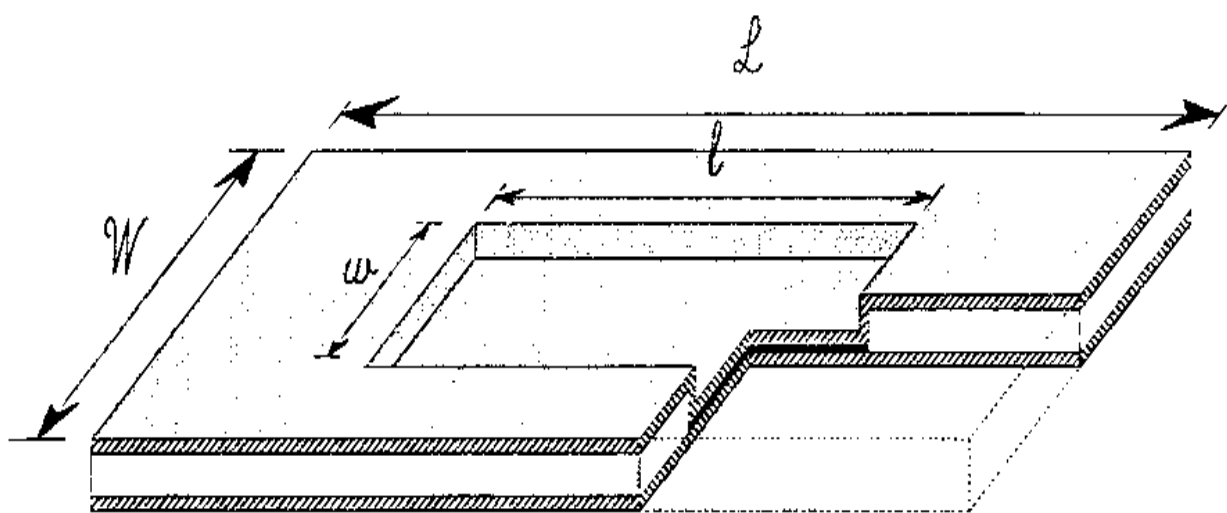
For a number of points in x and y , $M = 100$, we obtain that the energy is conserved up to 10^{-3} in relative error for $t < 1$.

FIGURE CAPTIONS

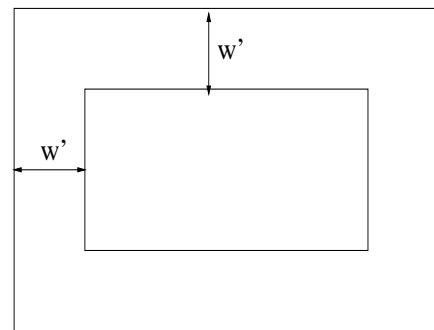
- 1 Top panel: a view of a window Josephson junction. The bottom left panel shows a schematic top view. For the system shown on the right the linear region exists only on the left and right sides of the junction.
- 2 Phase plane (X, u) for an antikink wave propagating across an interface at $x = 0$. The solid line presents the solution of the adiabatic equations (14-15) and the losanges are the numerical solution of the partial differential equation (10). The parameters are $\epsilon_0 = 0.6, \gamma = 0.02, L_I = 1$ (top panel) and $L_I = 1.5$ (bottom panel).
- 3 Interface between a nonlinear and linear medium, the top panel shows a plot of the antikink position $X(t)$ vs. time for the solution of the adiabatic equations (14-15) in full line. The crosses indicate the solution of the partial differential equation (10). The bottom panel presents the velocity $v(t)$. The parameters are $\epsilon_0 = 0.1, \gamma = 0.01, L_I = 1$.
- 4 Simplified description of the fluxon motion in a one dimensional window junction for $L_I \gg 1$ (top panel) and $L_I \ll 1$ (bottom panel). The stable fixed points are shown by the large circles and the unstable ones are the small circles.
- 5 Motion of a fluxon in a one dimensional window junction from the numerical solution of (10). The top and middle panels show respectively the position $X(t)$ and velocity $u(t)$ vs. time while the bottom panel shows the phase plane (X, u) . The parameters are $\epsilon_0 = 0, w' = 2, L_I = C_I = 2, I = 0.1..$
- 6 Contour plot of the phase $\varphi(x, y, t)$ for $t = 0, 400, 600, 800$ of the numerical solution of the two dimensional window junction equations (1). The parameters are the same as in Figure 5.
- 7 Contour plots of the phase $\varphi(x, y, t)$, numerical solution of (1) for $t = 0, 5, 6$ and 8 clockwise starting from the top left panel. The parameters are $w' = 7, L_I = C_I = 1, I = 0.3$.
- 8 Plots of the phase $\varphi(x, y, t)$, numerical solution of (1) for $t = 2, 10$ and 20 from left to right. The top panels show the contours while the bottom show the three dimensional plots. The parameters are $w' = 2, L_I =$

0.0001, $C_I = 1, I = 0.3$.

- 9 Contour plots of the phase $\varphi(x, y, t)$, numerical solution of (1) for $t = 50100$ (top) and 51000 (bottom) from left to right. The parameters are the same as in Fig. 8 except $L_I = 10000$.
- 10 Parameter plane (L_I, C_I) showing the regions of existence of zero field steps (ZFS) corresponding to the shuttling motion of a fluxon. The velocities v_I are indicated in the top right corner of the picture.



1D



2D

Fig.1 , Benabdallah et al

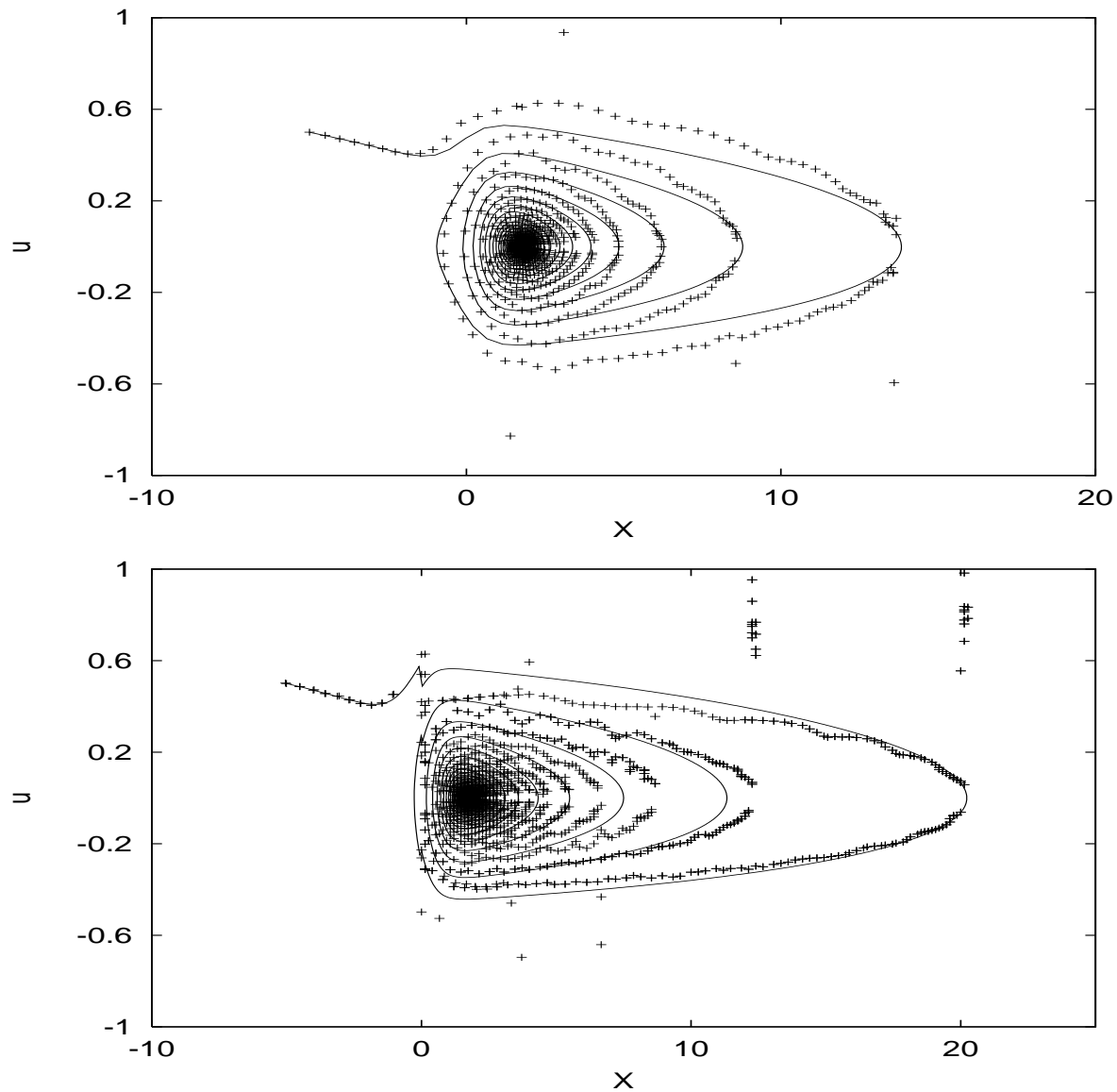


Fig. 2 , Benabdallah et al

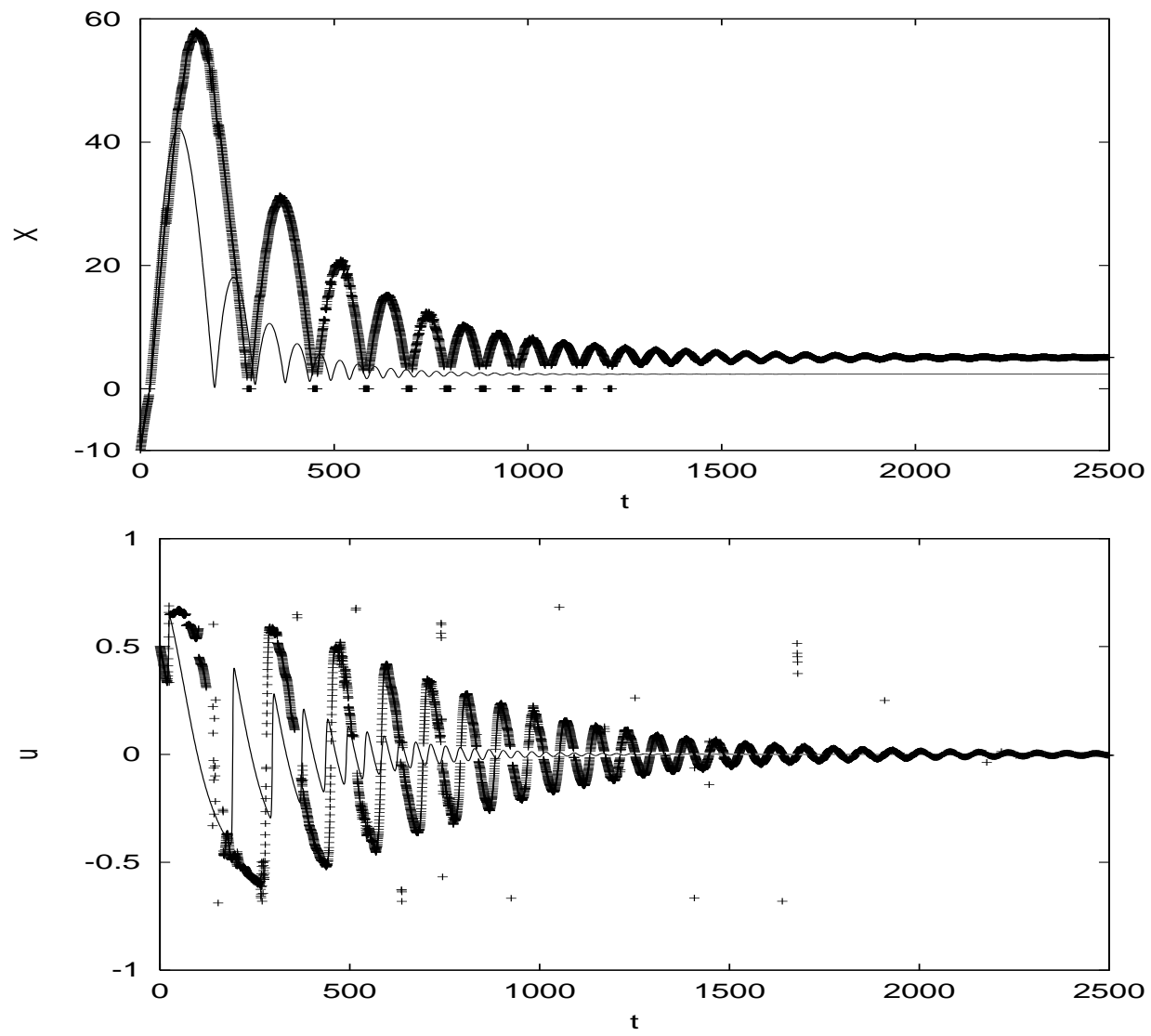


Fig. 3 , Benabdallah et al

Large inductance



kink



small inductance



kink

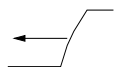


Fig. 4 , Benabdallah et al

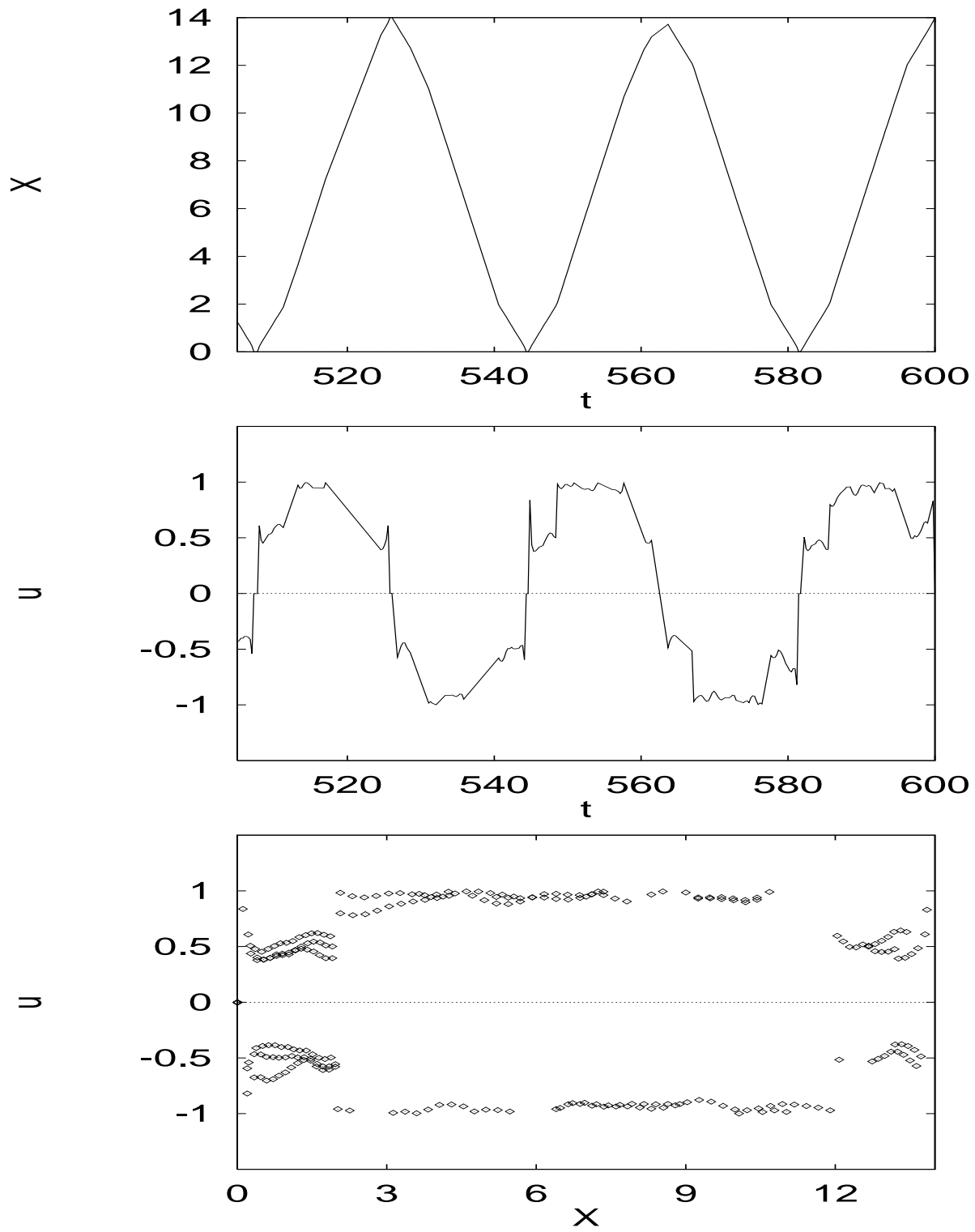


Fig. 5 , Benabdallah et al

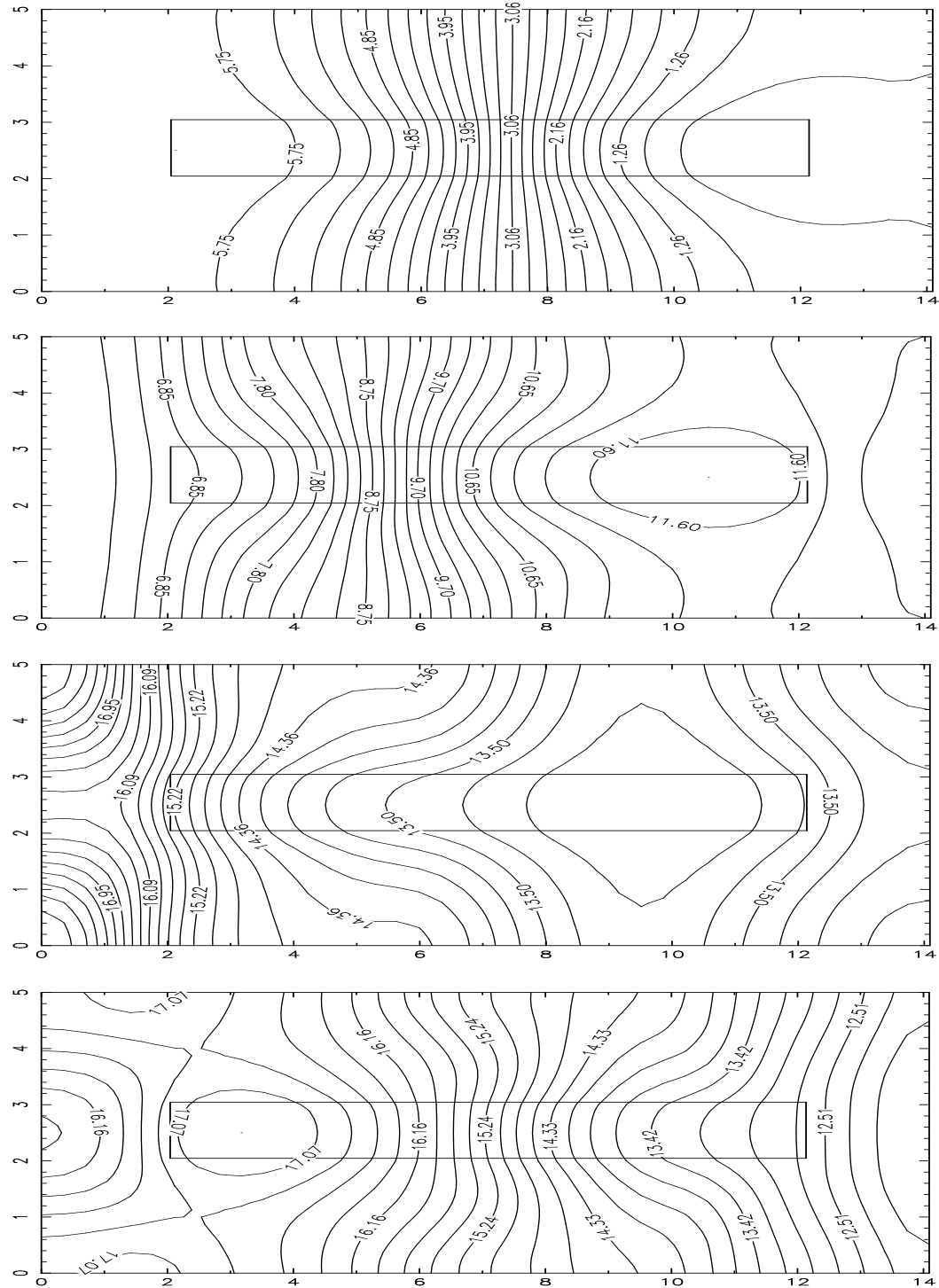


Fig. 6 , Benabdallah et al

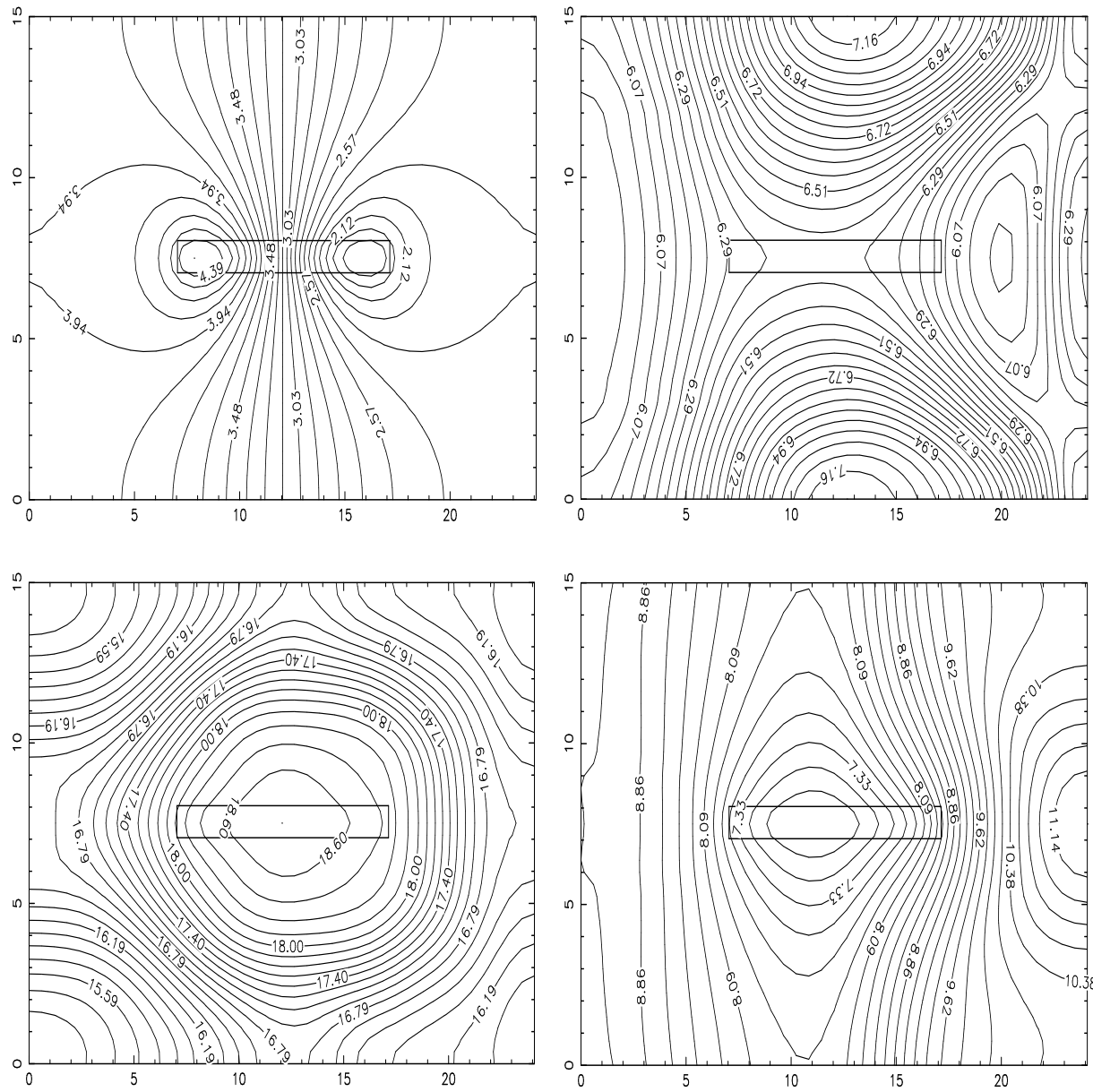


Fig. 7 , Benabdallah et al

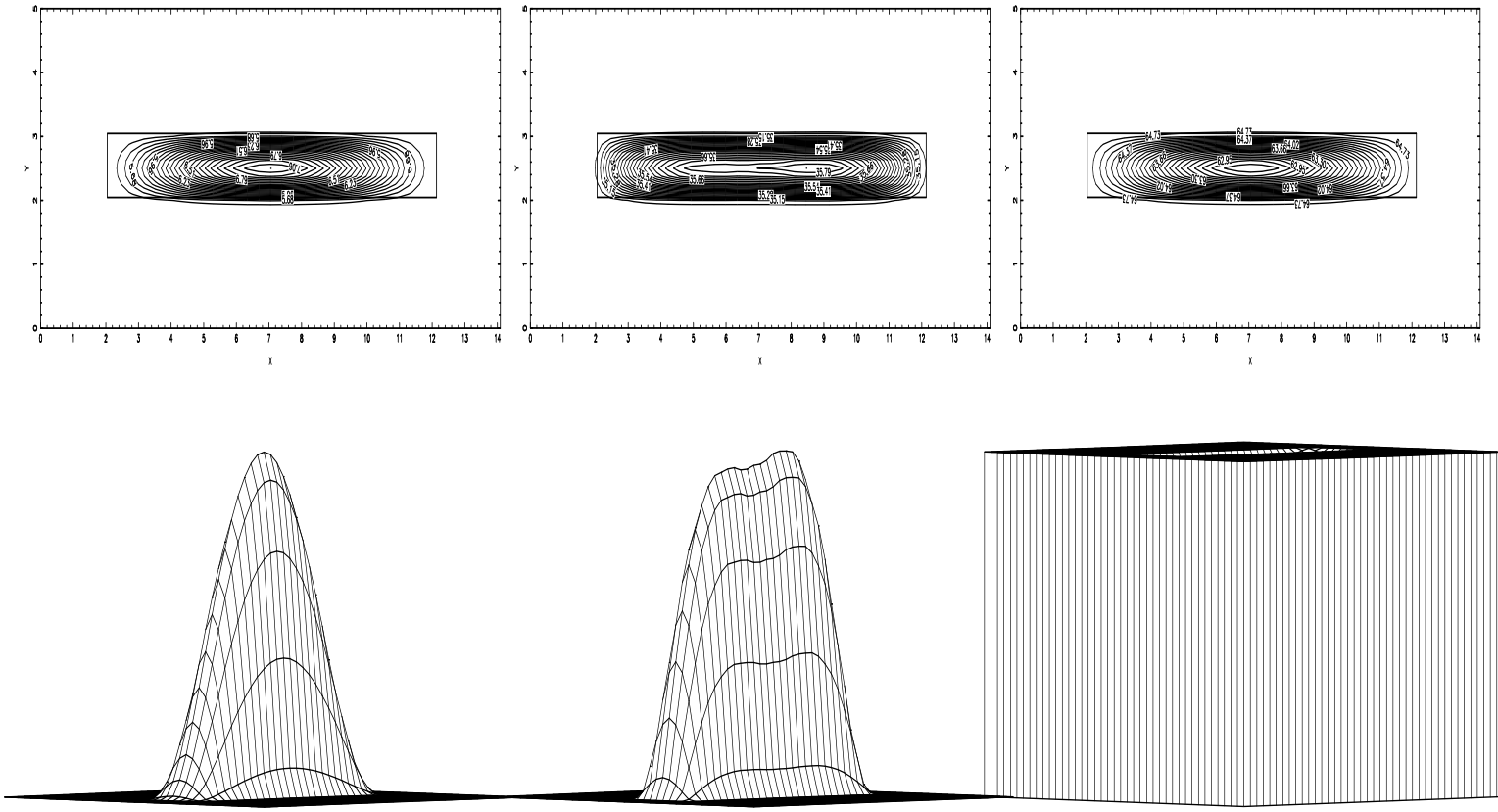


Fig. 8 , Benabdallah et al

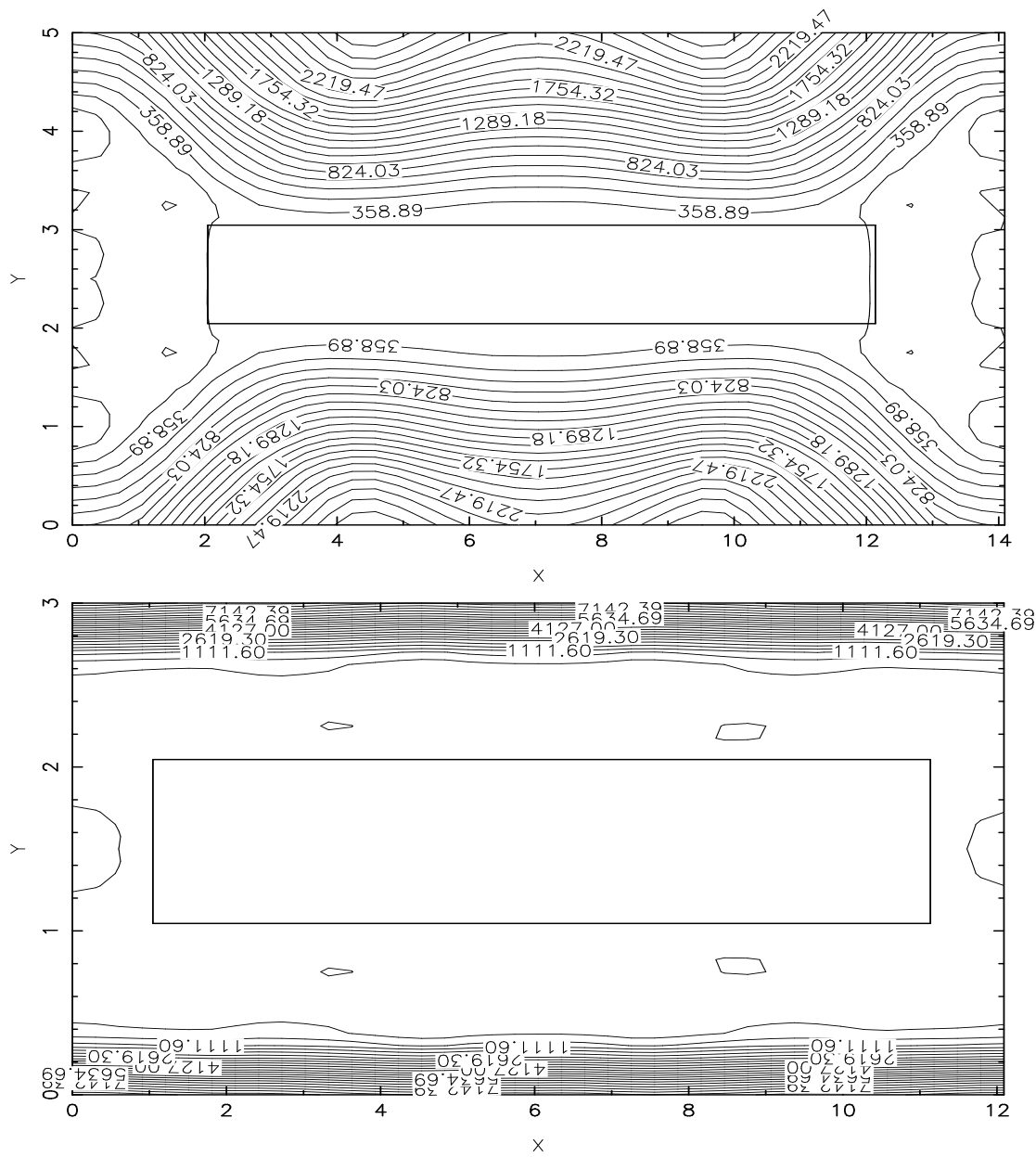


Fig. 9 , Benabdallah et al

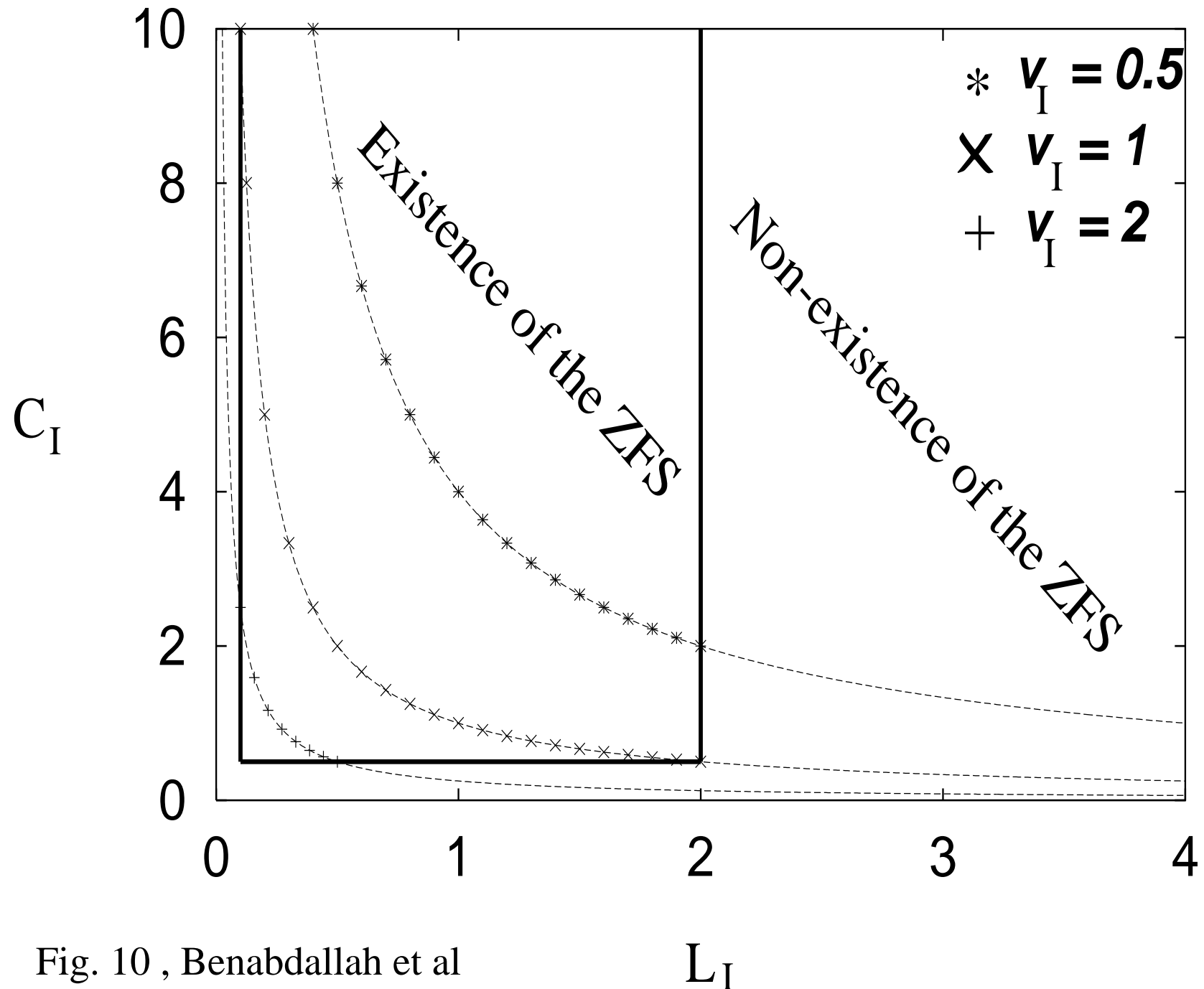


Fig. 10 , Benabdallah et al

L_I